

1

2

This manuscript has been submitted for publication in *Geophysical Research Letters*.

3

Please note that, despite being peer-reviewed, the manuscript has yet to be formally

4

accepted for publication. Subsequent versions of this manuscript may have slightly

5

different content. If accepted, the final version of this manuscript will be available via the

6

'Peer-reviewed Publication DOI' link on the right-hand side of this webpage. Please feel

7

free to contact any of the authors; we welcome feedback.

8

9

A minimally cemented shallow crust beneath InSight

10

Vashan Wright¹, Jhardel Dasent¹, Richard Kilburn¹, and Michael Manga²

11

¹University of California San Diego, Scripps Institution of Oceanography, La Jolla, CA, 92037

12

²University of California Berkeley, Department of Earth and Planetary Science, Berkeley, CA, 94720

13

Key Points:

14

- Any significant volumes of ice or mineral cements within the upper 300 m beneath InSight are likely nodular or broken.

15

16

- No ice- or liquid water-saturated layers were seismically resolved within the upper 300 m beneath InSight.

17

18

- Up to 20% ice is permissible within the pores of fractured basalt layers in the upper 300 m beneath InSight.

19

Corresponding author: Vashan Wright, vwright@ucsd.edu

Abstract

Ice and other mineral cements in Mars' shallow subsurface affect the mechanical properties of the shallow crust, the geologic processes that shape the planet's surface, and the search for past or extant Martian life. Cements increase seismic velocities. We use rock physics models to infer cement properties from seismic velocities. Model results confirm that the upper 300 m of Mars beneath InSight is most likely composed of sediments and fractured basalts. Grains within sediment layers are unlikely to be cemented by ice or other mineral cements. Hence, any existing cements are nodular or formed away from grain contacts. Fractures within the basalt layers could be filled with gas, 2% mineral cement and 98% gas, and no more than 20% ice. Thus, no ice- or liquid water-saturated layers likely exist within the upper 300 m beneath InSight. Any past cement at grain contacts has likely been broken by impacts or marsquakes.

Plain Language Summary

Quantifying how much and where ice and other minerals exist within Mars' shallow subsurface may help to determine if Mars ever supported life, to understand its climate history, to understand Mars as a geological system, and to prepare for human exploration. The InSight lander on Mars has an instrument whose data provide estimates for the velocity of seismic waves within the crust. These velocities change depending on rock type and the material that fills the pores within rocks. Possible pore-filling materials include gas, liquid water, ice, and other mineral cements. We find that the shallow crust is at best weakly cemented and the pores within the rocks are not entirely filled with ice or liquid water.

1 Introduction

Cements in the Martian crust can have multiple origins, including ice frozen from liquid water or condensed from vapor, hydrated minerals formed in situ, or minerals precipitated from aqueous fluids (e.g., salts, carbonates, and sulfates). The presence, amount, and composition of ice and other mineral cements in the shallowest sections of the Martian crust have implications for robotic and human exploration of Mars, the processes that shape and shaped the surface, and the search for past or extant life. Research on these topics is central to determining if Mars ever supported life, to understand the climate history and processes, to understand Mars as a geological system, and to prepare for human exploration.

Cementation affects and records geological processes. Cement can strengthen sediments (herein defined to include regolith and all other granular media layers) by creating stiffer contacts between particles. Cementation affects the permeability and porosity of sediments and fractured rocks, which impacts gas transport driven by atmospheric pressure changes (Morgan et al., 2021). Pores and fractures filled with ice or other mineral cement could confine any deeper liquid water, creating aquifers (Carr, 1979). Ground ice can promote weak explosive eruptions at rootless cones on lava flows (Brož et al., 2021) and may promote phreatomagmatic eruptions (Moitra et al., 2021). Cemented sediments are less prone to eolian and fluvial transport and erosion. The distribution of cements in the Martian sediments may record the accumulation and transport of volatiles in geologically recent times (Dundas et al., 2021). Cements may also preserve organic compounds diagnostic of past or present biological activity (Rivera-Valentín et al., 2020).

Cementation impacts human exploration, and a primary motivation for the Mars Ice Mapper mission concept is to map ice in the shallowest crust (Davis & Haltigin, 2021). The presence of ice and hydrated minerals in shallow sediments and fractured rocks could provide a source of water for in situ resource utilization (Piqueux et al., 2019). Cementation-

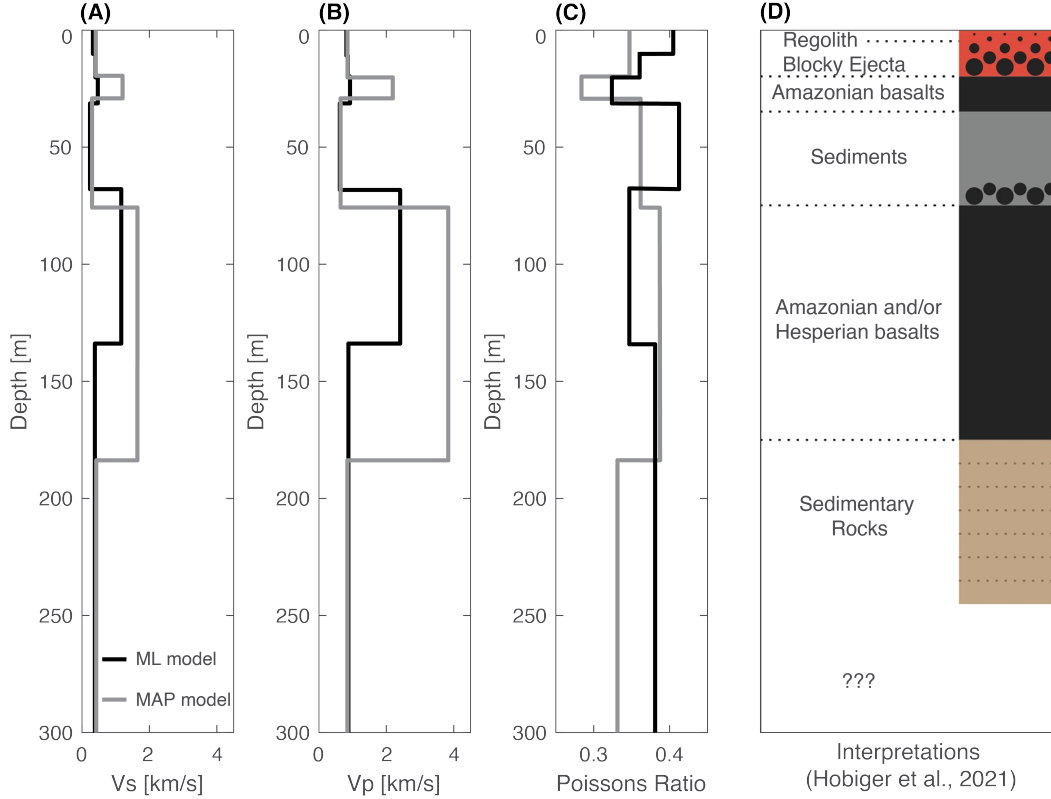


Figure 1. Models of (A) V_s and (B) V_p from Hobiger et al. (2021) and (C) calculated Poisson's ratio based on the seismic velocities. The black and grey curves are Hobiger et al. (2021)'s maximum likelihood (ML) and maximum a posteriori (MAP) models, respectively. (D) Inferred stratigraphy of the upper 300 m beneath InSight, from Hobiger et al. (2021).

68 induced strengthening of sediments affects foundations used for engineering infrastruc-
 69 ture (Kalapodis et al., 2020). Cemented sediments can be used as a construction ma-
 70 terial (Liu et al., 2021) and have prompted studies of a range of Mars simulants in prepa-
 71 ration for future human missions (Karl et al., 2021).

72 Efforts to map and study shallow subsurface ice and other mineral cements inte-
 73 grate complementary insights from direct and indirect observations. Direct, in situ mea-
 74 surements of ice and other mineral cements at specific landing sites are possible, yet some-
 75 times challenging. The Phoenix lander excavated ice in the upper few cm (Morgan et
 76 al., 2021). Eolian processes and impact brecciation created a 10-30 m thick regolith (in-
 77 cluding a sand horizon in the upper 3 m) at the InSight (Interior Exploration using Seis-
 78 mic Investigations, Geodesy, and Heat Transport mission) landing site (Golombek et al.,
 79 2020; Warner et al., 2022). There, the rover had difficulties penetrating its heat flow probe
 80 (HP3) into the subsurface owing to insufficient friction (Spohn et al., 2022). Indirect meth-
 81 ods of detecting ice and other mineral cements include analyses of neutron detection, ther-
 82 mal inertia, geomorphic, and radar data (Morgan et al., 2021). Other indirect methods
 83 exploit the sensitivity of geomechanical properties to cements, which influence geophys-
 84 ical properties such as seismic velocity, electrical conductivity, and gravity. For exam-
 85 ple, Manga and Wright (2021) used seismic velocities interpreted with rock physics mod-
 86 els for fractured rocks to infer that there is likely no ice-saturated cryosphere in the 0
 87 to 7.5 km depth range beneath the InSight landing site, though they suggested that some
 88 mineral cement could be present at greater depths.

Here we study the presence and quantity of mineral and ice cements in the upper 300 m of the Martian crust by interpreting seismic velocity models derived from data collected by the seismometer deployed by the InSight lander. We interpret the seismic velocities using rock physics models for both fractured rocks and sediments. We also interpret seismic velocities using a theoretical relationship between dry-frame Poisson's ratio and grain contact forces in sediments. Figure 1 based on results from Hobiger et al. (2021) shows their derived seismic velocities beneath InSight and the inferred stratigraphy and lithology. Shear wave velocities V_s generally increase from ~ 0.3 km/s at the surface to ~ 1.7 km/s at 175 m; compressional wave velocities V_p increase from ~ 0.8 km/s to ~ 3.8 km/s within the same depth. At least two low velocity zones exist from 0-157 m and 175-300 m, where V_s decreases to ~ 0.4 km/s and V_p decreases to ~ 0.8 - 0.9 km/s. Hobiger et al. (2021) interpreted the higher and lower velocity layers as fractured basalts and sediment, respectively (Figure 1D), consistent with geological mapping (Warner et al., 2022). Our interpretations of these seismic velocities are that sediments within the upper 300 m of the Martian crust is gas-filled; mineral or ice cements likely do not exist at grain contacts and there is no evidence for any ice-saturated cryosphere.

2 Methods

2.1 Inferring Subsurface Properties Using Rock Physics Models

We compare measured with theoretically modeled V_s and V_p to infer the mechanical properties of the upper 300 m beneath InSight, constraining uncertainties with Monte Carlo analyses. For sediments, we assume a porosity reduction profile for Mars, predict seismic velocities with that assumed profile, then compare modeled to measured velocities within the lower velocity zones. For fractured basalt layers, we create rock physics templates that relate seismic velocities, porosity ϕ (0-50%), and fracture shape represented by elliptical inclusions with an aspect ratio, defined as the short axis divided by long axis, $\alpha = 0.01$ - 1 . We use the templates to identify the combinations of porosity and fracture shapes that could explain both measured V_p and V_s within the higher velocity zones.

We compute V_s and V_p from

$$V_s = \sqrt{\frac{\mu_e}{\rho}} \quad (1)$$

$$V_p = \sqrt{\frac{\kappa_e + \frac{4}{3}\mu_e}{\rho}} \quad (2)$$

where ρ , κ_e , and μ_e are bulk density, effective bulk modulus, and effective shear modulus, respectively. Bulk density ρ is

$$\rho = \sum_i \phi_i \rho_i \quad (3)$$

where ρ_i and ϕ_i are densities and volume fractions of the i^{th} constituents, respectively.

Rock physics theoretical models predict dry-frame shear and bulk moduli (μ and κ); $\mu_e = \mu$ and $\kappa_e = \kappa$ for dry rock (Gassmann, 1951; Biot, 1956). We use Hertz-Mindlin's (Mindlin, 1949) rock physics models for uncemented sediments. We use the contact cement model (Dvorkin & Nur, 1996) for sediments with cement that completely surrounds grains that are in contact or cement that only exists at grain contacts. We use the Berryman self-consistent model (Berryman, 1980) for fractured rocks. The equations for the rock physics models are in Mindlin (1949), Dvorkin and Nur (1996), and Berryman (1980).

128 We use Gassmann-Biot fluid substitution theory (Gassmann, 1951; Biot, 1956) to
 129 calculate effects of fluid saturation on κ (i.e., κ_e for liquid water saturated rocks),

$$\frac{\kappa_e}{\kappa_m - \kappa_e} - \frac{\kappa_{f2}}{\phi(\kappa_m - \kappa_{f2})} = \frac{\kappa}{\kappa_m - \kappa} + \frac{\kappa_{f1}}{\phi(\kappa_m - \kappa_{f1})} \quad (4)$$

130 where κ_{f2} , κ_m , and κ_{f1} are the bulk moduli of the saturating fluid (liquid water in our
 131 case), mineral(s), and gas (0 kPa), respectively. Gassmann-Biot theory assumes that flu-
 132 ids are not flowing and minerals and fluids homogeneously distribute within rocks (Gassmann,
 133 1951; Biot, 1956).

134 The models' input parameters are porosity ϕ , coordination number c_n (average num-
 135 ber of grains in contact), effective pressure P , mineral Poisson's ratio ν_m , cement frac-
 136 tion c_f , mineral bulk κ_m and shear μ_m moduli, pore aspect ratio α , and grain rough-
 137 ness fraction f (i.e., percentage of grain contacts that allows tangential slip, which we
 138 assume to be 0 % or 100 % to model end-member ranges). We assume porosity ϕ at the
 139 surface (critical porosity ϕ_c) is between 0.3 and 0.5 (Golombek et al., 2018; Lewis et al.,
 140 2019; Smrekar et al., 2019; Lognonné et al., 2020) and that ϕ exponentially decays with
 141 depth z ,

$$\phi = \phi_c e^{-\frac{z}{k}} \quad (5)$$

142 where k is a compaction constant (2.82 km) scaled to Mars' gravitational field (Clifford,
 143 1986). Effective pressure P is

$$P = \rho gh - p_f \quad (6)$$

144 where g , h , and p_f represent Mars' gravitational acceleration (3.71 m/s²), depth, and
 145 fluid pressure, respectively. We constrain coordination number c_n empirically (Murphy,
 146 1982)

$$c_n = 20 - 34\phi + 14\phi^2. \quad (7)$$

147 The minerals that we use in the models and their respective κ_m and μ_m in GPa are cal-
 148 cite cement (71.6 and 28.2), basalt grains and rocks (80.0 and 40.0), and ice cement (8.7
 149 and 3.8) (Vanorio et al., 2003; Zong et al., 2017). These are some of the main minerals
 150 expected within the upper 300m of the Martian crust (Tanaka et al., 2014; Golombek
 151 et al., 2018; Pan et al., 2020); we also consider other cements listed in Table S1. We cal-
 152 culate mineral Poisson's ratio from

$$\nu_m = \frac{3\kappa_m - 2\mu_m}{6\kappa_m + 2\mu_m}. \quad (8)$$

153 We use Monte Carlo analyses to constrain the effects of input parameter uncertain-
 154 ties on the velocities predicted by the rock physics model for cemented and uncemented
 155 sediments. In each of our 10,000 realizations, we randomly generate and use a new in-
 156 put parameter value between their ranges. We generate new ϕ -depth profiles from the
 157 selected ϕ_c . Coordination numbers, bulk densities, and effective pressures change with
 158 ϕ -depth profiles.

159 2.2 Inferring Subsurface Properties From Poisson's Ratio

160 We infer the volume fraction of cemented grain contacts from the relationship be-
 161 tween Poisson's ratio ν_d and f , the volume fraction of rough versus smooth grain con-
 162 tacts. Rough (smooth) grain contacts resist (allow) elastic tangential grain contact slip
 163 during seismic wave propagation. We conjecture that, in the absence of cemented grains,

164 Martian sediments comprise nearly 100% smooth grain contacts. We make this con-
 165 jecture because Mars' gravitational acceleration (3.7 m/s^2) is lower than Earth's (9.8 m/s^2).
 166 Gravitational acceleration impacts grain contact forces significantly (Equation 6). As-
 167 suming 100% smooth grain contacts routinely results in better seismic velocities predic-
 168 tions in shallow sediments on Earth (up to 600 m below the surface in some cases) (Buckingham,
 169 2000; Zimmer et al., 2007; Majmudar & Behringer, 2005; Wright & Hornbach, 2021). Low
 170 friction at grain contacts, despite cohesion and possibly partial cementation, appears to
 171 have prevented InSight's heatflow probe from penetrating the shallow subsurface (Spohn
 172 et al., 2022). Given the assumptions, conjectures, and expectations mentioned, cements
 173 are likely one of the main causes for rough grain contacts, making f synonymous with
 174 the volume of cemented grain contacts in those cases. We compute f from ν_m and ν_d
 175 for an aggregate of identical perfect spheres (Walton, 1987; Bachrach & Avseth, 2008)

$$\nu_d = \frac{(2 - \nu_m)}{4(2 - \nu_m) + 2f(1 - \nu_m)} - \frac{2f(1 - \nu_m)}{4(2 - \nu_m) + 2f(1 - \nu_m)}. \quad (9)$$

176 f decreases as ν_d increases (Walton, 1987). We compute ν_d from the measured V_p and
 177 V_s

$$\nu_d = \frac{1}{2} \frac{(V_p/V_s)^2 - 2}{V_p/V_s)^2 - 1}. \quad (10)$$

178 Our calculation assumes that there is no liquid water within the sediment layers.

179 3 Results

180 3.1 Inferred Pore-Filling Media in Sediments

181 The sediment layers most likely host grains that experience relatively low friction
 182 at contacts. Low friction is indicated by the observation that smooth-grained models pro-
 183 duce better seismic velocity predictions (i.e., lower misfits) than rough-grained models,
 184 regardless of assumed pore-filling material (Figure 2). The differences between smooth-
 185 versus rough-grain model predictions are 0.3-0.4 km/s and 0.1-0.5 km/s for V_s and V_p ,
 186 respectively. Low friction is also indicated by the Poisson's ratio for sediment layers, 0.33-
 187 0.41 (Figure 1). These Poisson's ratio values result in negative values (-0.55 to -0.10) for
 188 the calculated volume fraction of rough grains (equation 10), which indicates that there
 189 are likely no rough grain contacts present, that the model breaks down for such high val-
 190 ues or both.

191 The pores within the sediment layers are most likely filled with gas (Figure 2). Mod-
 192 eled smooth-grained V_s for gas and liquid water-filled pores are within 0-0.1 km/s of mea-
 193 sured V_s . Modeled V_p are within 0.01-0.05 km/s of measured V_p , assuming that gas fills
 194 the pores; assuming 100% liquid water in the pores results in V_p overprediction by 0.6-
 195 1.0 km/s. Models that assume pores are filled with 2% cement overpredict V_p and V_s by
 196 1.4-3.0 km/s. Assuming that ice fills the pores results in V_p and V_s overpredictions by
 197 2.3-3.2 km/s and 1.7-2.4 km/s, respectively for the sediments.

198 3.2 Inferred Pore-Filling Media in Fractured Basalts

199 The hypothesized fractured basalt layers could host 100% gas, 100% liquid water,
 200 2% calcite cement and 98% air, or 2% calcite cement and 98% water in the fractures;
 201 hosting 100% ice is unlikely. A gas-filled basalt requires the narrowest range of aspect
 202 ratio and porosity combination to be consistent with the measured seismic velocities. A
 203 liquid water-filled basalt is consistent with the measured seismic velocities if the basalts'
 204 porosities are between 0.13 and 0.47 for aspect ratios between 0.03 and 1; aspect ratios
 205 increase with increasing porosities. A basalt hosting 2% calcite cement and 98% gas or
 206 liquid water in its fractures could explain the measured velocities if the porosities are
 207 0.24-0.5. The range of possible aspect ratios increases with increasing porosities. All com-
 208 binations of porosities and aspect ratios for a 100% ice-filled basalt results in velocities

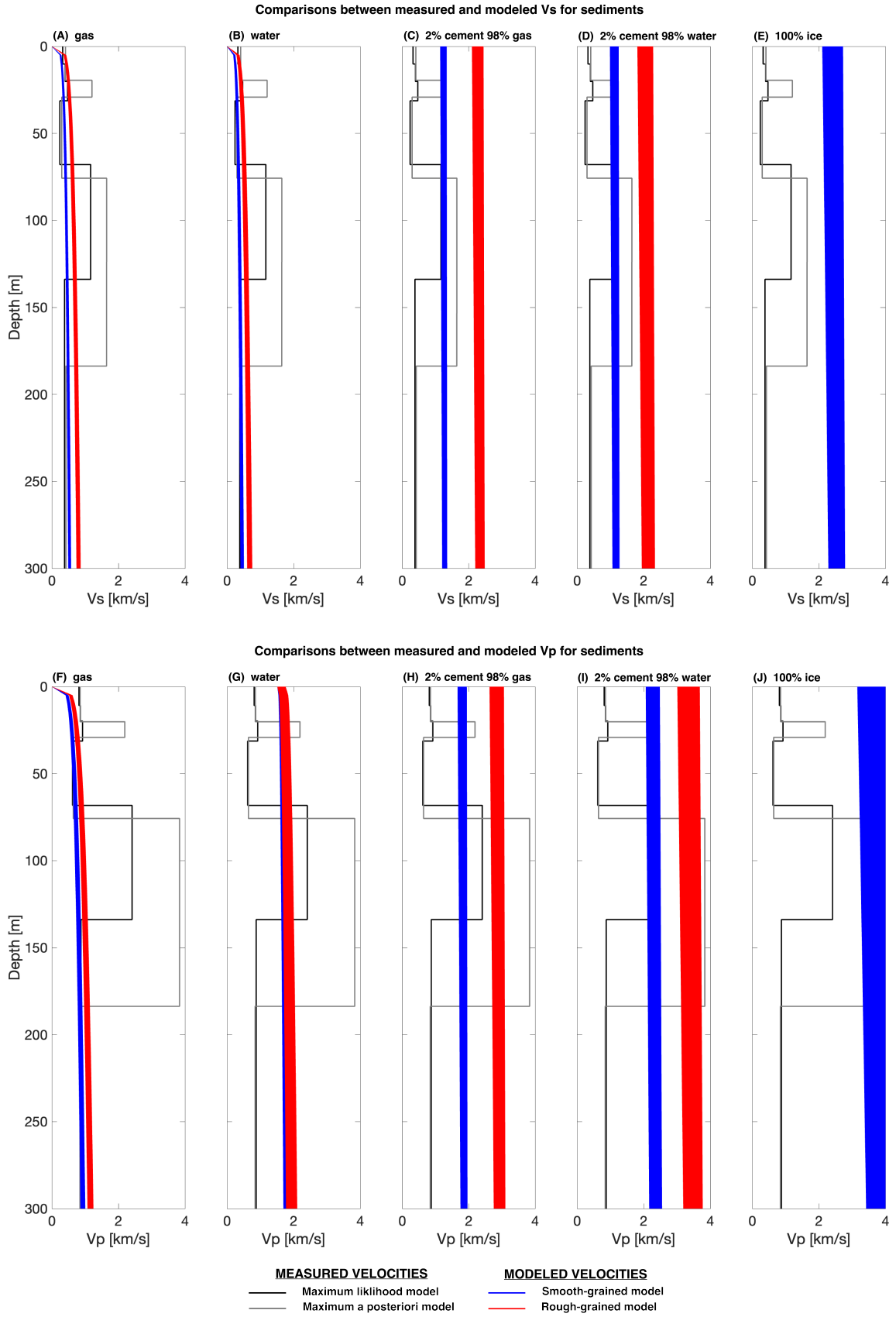
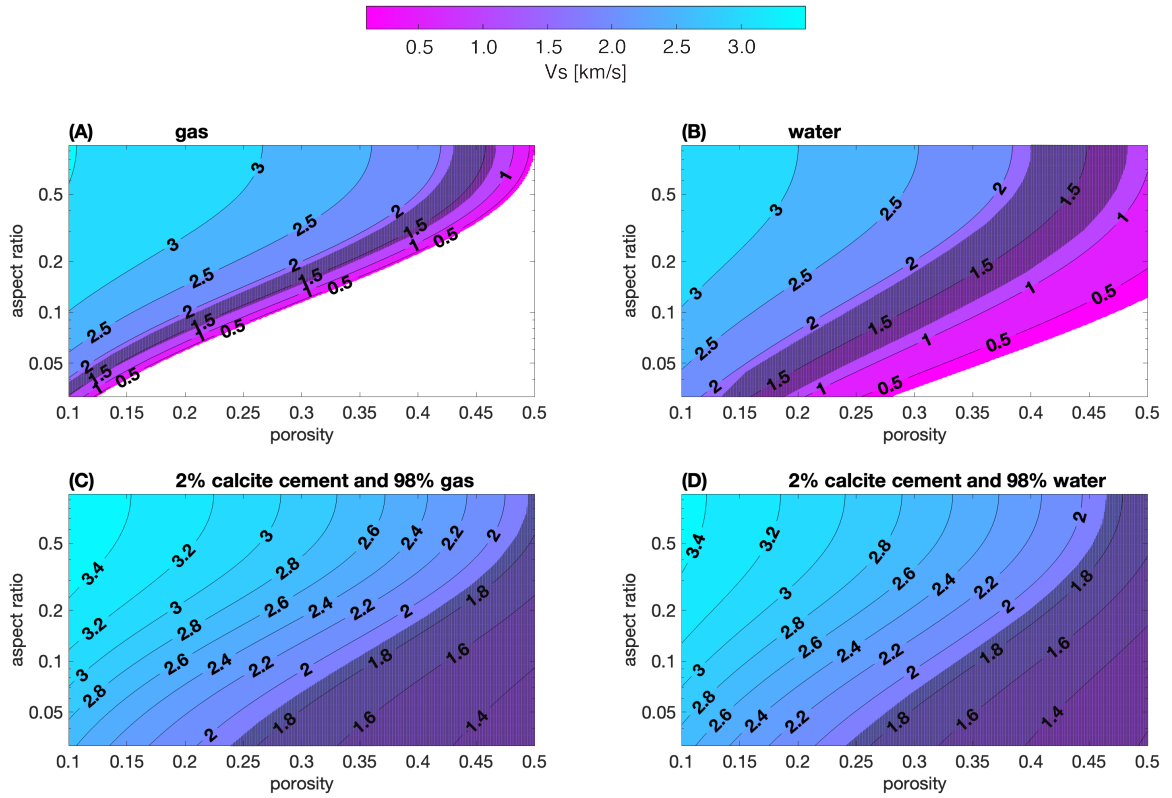


Figure 2. Measured V_p and V_s (black and grey lines) compared to model predicted V_p and V_s for sediment whose pores are filled with gas, liquid water, 2% calcite cement and 98% gas, 2% calcite cement and 98% liquid water, and ice. Blue and red lines are the smooth-grained and rough-grained model results, respectively.

Comparisons between measured and modeled V_s for fractured basalts with varying pore-filling media



Comparisons between measured and modeled V_p for fractured basalts with varying pore-filling media

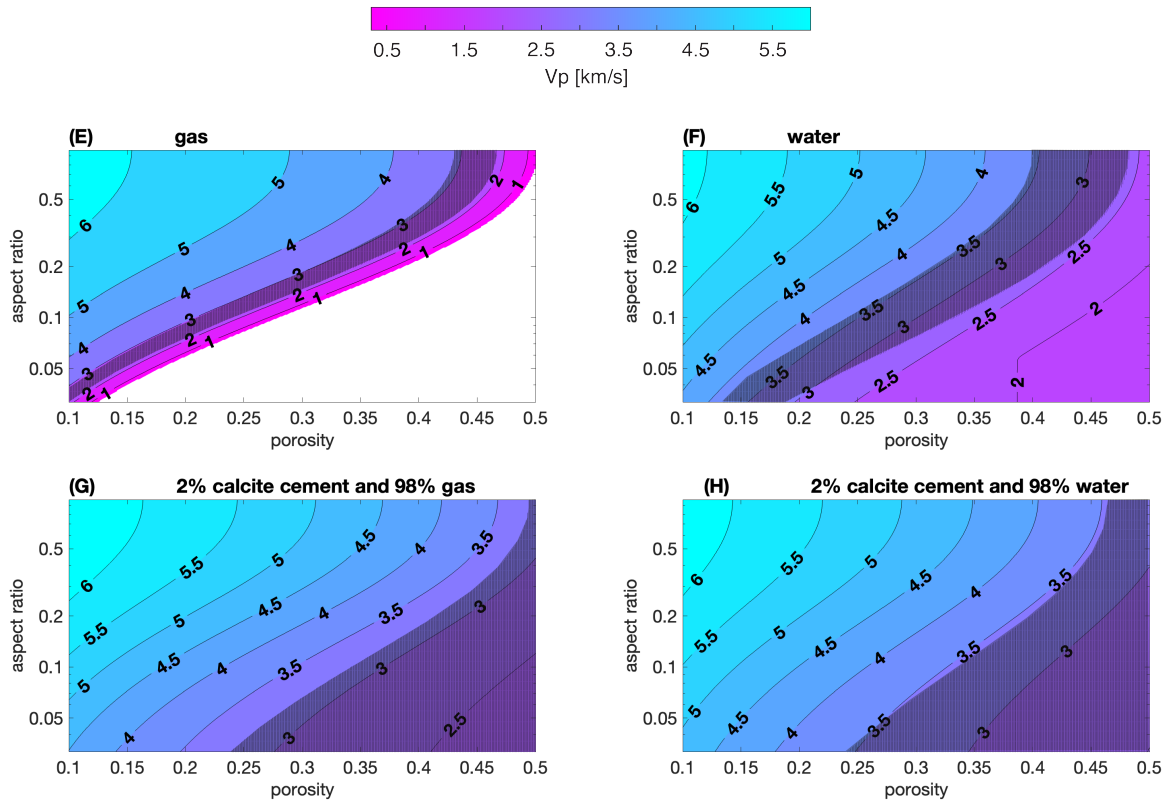


Figure 3. Rock physics model templates showing predicted V_s and V_p for a fractured basalt with various pore-filling materials. Shaded regions are the combinations of modeled velocities, porosities, and aspect ratios that match both the measured V_p and V_s for the higher velocity zones. Vertical scale is logarithmic.

209 that are 1.1-2.8 times higher than measured. Thus, measured V_s and V_p are too low for
 210 a 100% ice-filled fractured basalt.

211 4 Discussion

212 We now discuss our most robust interpretations for the distribution of cements within
 213 the upper 300 m beneath InSight, considering the model assumptions and limitations.
 214 The cemented and uncemented granular media models assume that grains are identical
 215 spheres experiencing equal contact forces, which are idealizations for Martian and other
 216 sediments (Makse et al., 1999, 2004; Day-Lewis et al., 2005; Majmudar & Behringer, 2005;
 217 Bachrach & Avseth, 2008). These model assumptions sometimes lead to overpredictions
 218 in low effective stress environments on Earth (Buckingham, 2000; Zimmer et al., 2007;
 219 Majmudar & Behringer, 2005; Wright & Hornbach, 2021). The cementation models pre-
 220 dict elastic moduli by homogeneously distributing the entire volume of cement within
 221 the sediments, which may also be too idealistic for actual sediments (Dvorkin & Nur,
 222 1996). Considering the model limitations, we can still make two main interpretations:
 223 any shallow cements in Martian sediments likely do not adhere grains, and pores within
 224 the layers are not filled with liquid water or ice.

225 4.1 Fractured Basalt Layers with up to 20% of its Pores Filled with Ice

226 A seismically detectable cryosphere likely does not exist within the upper 300 m
 227 beneath InSight. This is indicated by the observation that the granular and fractured
 228 media models predict velocities that are too high for fully ice-saturated sediments and
 229 basalt. Manga & Wright (2021) drew a similar conclusion for the upper 8 km of crust
 230 because their modeled V_s for an ice-saturated basalt was low compared to measured V_s .
 231 It is unlikely that we misinterpreted a basalt layer for an ice-saturated sediment layer;
 232 the predicted V_p for the Amazonian and/or Hesperian basalt layer matches, but V_s is
 233 overpredicted by at least 0.5-2.3 km/s (Figures 1-2). A partial cryosphere, with up to
 234 20% ice, could exist in the fractured basalt layers. Though the measured velocities are
 235 consistent with modeled velocities for a fractured basalt whose pores are filled with up
 236 to 40% ice, porosities of basaltic lava flows rarely reach such high values except in thin
 237 horizons where vesicles accumulate (Cashman & Kauahikaua, 1997) or when chemical
 238 reactions alter the minerals within the basalt and lead to higher porosities (Franzson et
 239 al., 2010; Broglia & Ellis, 1990). Moreover, estimated and modelled porosity for exposed
 240 Martian basalts and meteorites are less than 40% (Hanna & Phillips, 2005; MacKinnon
 241 & Tanaka, 1989). Limiting the range of porosity to up to 40% then implies that mea-
 242 sured velocities are only consistent with a basalt with less than 20% of the pores filled
 243 with ice. We did not model the effects of salinity on ice and seismic velocities; increased
 244 salinity may lead to mushy ice in the pores and reduce seismic velocities, depending on
 245 the temperatures and wetting behavior (Dou et al., 2017). We also did not consider crustal
 246 V_s anisotropy, which may be used to constrain the orientation of cracks (Li et al., 2022).
 247 Future studies could explore these possibilities.

248 Our inferences are consistent with findings from the Mars Subsurface Water Ice Map-
 249 ping (SWIM) project, which used neutron detection, thermal inertia, geomorphology, radar
 250 surface mapping, and radar dielectric analysis to search for shallow subsurface ice (Morgan
 251 et al., 2021). The SWIM data compilation suggests that shallow ice is unlikely to be present
 252 at the near-equatorial landing site of InSight, 4.5 °N. SWIM is most sensitive to the up-
 253 per few meters, though radar reflection can probe depths greater than 100 m. Our find-
 254 ing that the shallowest sediment layer, which extends to 20-70 m, likely does not con-
 255 tain ice that cements grains is consistent with the SWIM map.

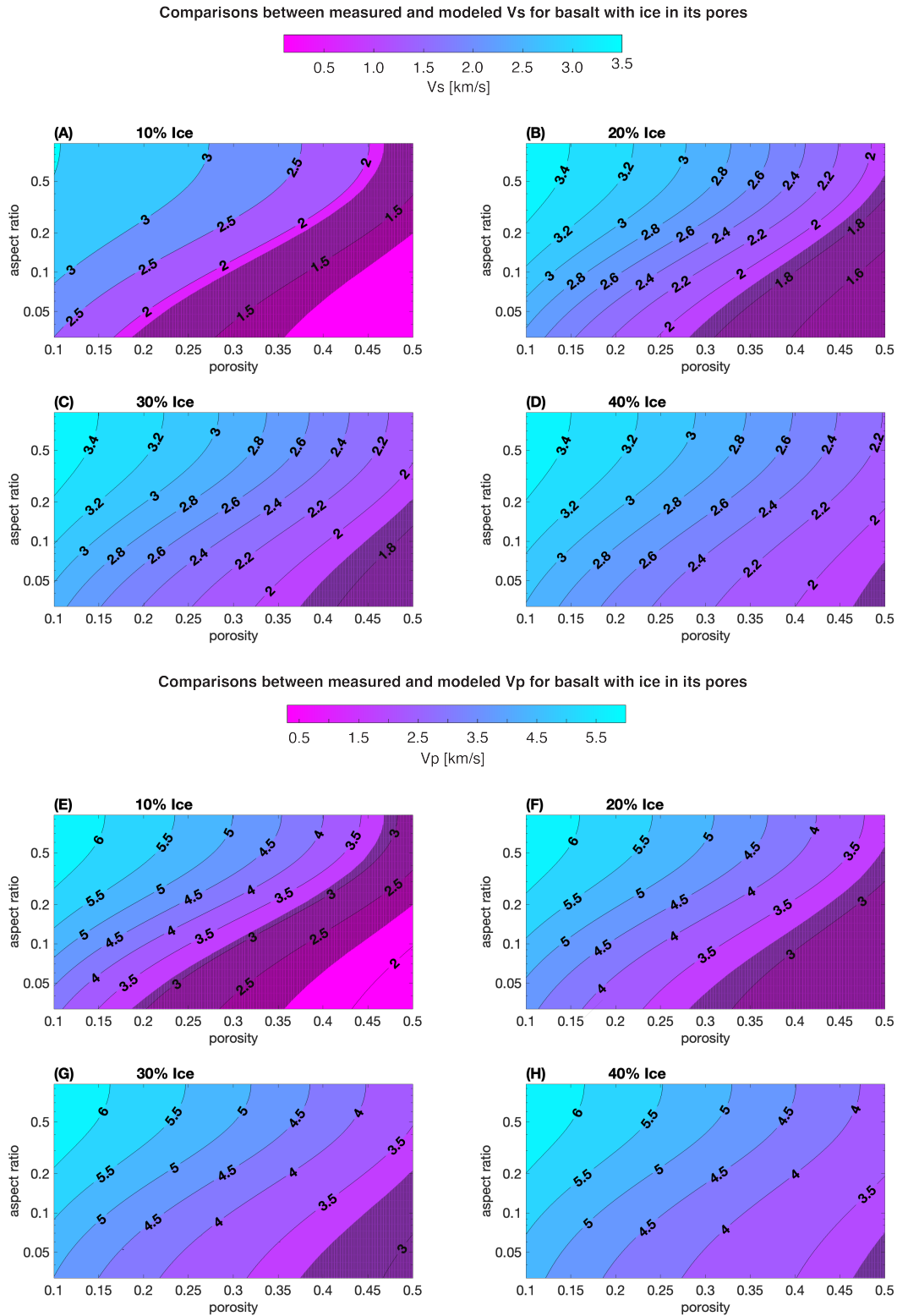


Figure 4. (A-H) Rock physics model templates showing predicted V_s and V_p for a fractured basalt with varying percentages of ice within the fractures. Shaded regions are the combinations of modeled velocities, porosities, and aspect ratios that match both measured V_s and V_p from Hobiger et al. (2021). Vertical scale is logarithmic. Figure S2 in the Supporting Information contains rock physics model templates showing predicted V_s and V_p for a basalt whose fractures are 50% and 100% filled with ice.

4.2 Mineral Cements as Framework Grains in Sediment Layers

Most mineral cements, if they exist, likely do not adhere grains substantially. Support for this interpretation comes from the observation that there are likely no significant volumes of rough grain contacts in sediments, as indicated by the high Poisson's ratios. Additional support comes from the observation that the models with calcite cement at grain contacts and surrounding the grains overpredict V_p and V_s by 1.4-3.0 km/s. Other mineral cements (e.g., halite, ice, gypsum, or kaolinite) also likely do not adhere grains since the differences in the elastic moduli between calcite and other mineral cements would not lead to a 1.4-3.0 km/s increase in seismic velocities (Figure S1). Nodular cements and concretions that are a part of the network of framework grains or cements that form on grains without adhering to other grains could exist. These cement types would produce roughly the same seismic velocities as gas-filled sediment with the same porosity. Thus, any existing cements likely resulted from mineral alteration, such as hydrating minerals (Scheller et al., 2021; Wernicke & Jakosky, 2021), precipitating salts (Sun et al., 2019), or the formation of concretions or spherules (Squyres et al., 2004, 2006).

Cements could have formed at the grain contacts of Martian sediments, only to be later broken by impacts and strong marsquakes. For example, the impacts that formed the large Noachian basins create dynamic strains similar to magnitude 10 and 11 quakes and could disrupt sediment globally on Mars (Clifford, 1997; Wang et al., 2005). Strains from smaller, local impacts and impact gardening of the surface might also disrupt cements in the younger Amazonian and Hesperian sediments and basalts in the upper few hundred meters. Laboratory experiments show that, depending on the porosity of the sediments and degree of cementation (weakly or strongly cemented), the relatively low strain rates from cyclic shearing (i.e., the type of waves experienced during seismic events) can break weakly cemented bonds (Sharma & Fahey, 2003; Zeghal & El Shamy, 2008; Suzuki et al., 2012; Suazo et al., 2017).

5 Conclusions

The presence, volume, and distribution of ice and other mineral cements in Martian sediments and fractured rocks may record and affect geologic processes. Seismic velocities are sensitive to cement properties, and rock physics models provide one approach to relate cement properties to seismic velocities. Using these models to interpret seismic velocities derived from InSight data, we find that any cement within the upper 300 m beneath InSight likely does not cement grain contacts in sediments. An ice-saturated sediment or fractured basalt layer likely does not exist, but fractured basalts whose pores contain up to 20% ice are possible. The findings support the ideas that some of Mars' past surface liquid water could be incorporated in cements that resulted from mineral alteration, precipitating salts, or the formation of concretions or spherules. Any cement at grain contacts was likely either weak and perhaps broken by impacts or marsquakes. Future studies could revisit these inferences as more constraints become available on the porosity, mineralogy, lithology, density, seismic velocity, and heat flow within the shallowest sections of the Martian crust.

6 Data Availability Statement

No new data was used in this study. The seismic velocity models are available in Hobiger et al. (2021).

Acknowledgments

302 Thanks to NASA and the InSight team for their vision, hard work, and dedication,
 303 especially during this time when Covid-19 is real. V. Wright, J. Dasent, and R. Kilburn
 304 acknowledge support from NSF grant EAR2136301. M. Manga acknowledges support
 305 from NASA grant 80NSSC19K0545 and the CIFAR Earth 4D program.

306 References

- 307 Bachrach, R., & Avseth, P. (2008). Rock physics modeling of unconsolidated sands:
 308 Accounting for nonuniform contacts and heterogeneous stress fields in the ef-
 309 fective media approximation with applications to hydrocarbon exploration.
 310 *Geophysics*, *73*(6), E197–E209. doi: <https://doi.org/10.1190/1.2985821>
- 311 Berryman, J. G. (1980). Long-wavelength propagation in composite elastic media II.
 312 Ellipsoidal inclusions. *The Journal of the Acoustical Society of America*, *68*(6),
 313 1820–1831. doi: <https://doi.org/10.1121/1.385172>
- 314 Biot, M. A. (1956). Theory of propagation of elastic waves in a fluid-saturated
 315 porous solid. II. Higher frequency range. *The Journal of the Acoustical Society*
 316 *of America*, *28*(2), 179–191. doi: <https://doi.org/10.1121/1.1908241>
- 317 Broglia, C., & Ellis, D. (1990). Effect of alteration, formation absorption, and
 318 standoff on the response of the thermal neutron porosity log in gabbros and
 319 basalts: Examples from Deep Sea Drilling Project-Ocean Drilling Program
 320 Sites. *Journal of Geophysical Research: Solid Earth*, *95*(B6), 9171–9188. doi:
 321 <https://doi.org/10.1029/JB095iB06p09171>
- 322 Brož, P., Bernhardt, H., Conway, S. J., & Parekh, R. (2021). An overview of ex-
 323 plosive volcanism on Mars. *Journal of Volcanology and Geothermal Research*,
 324 *409*, 107125. doi: <https://doi.org/10.1016/j.jvolgeores.2020.107125>
- 325 Buckingham, M. J. (2000). Wave propagation, stress relaxation, and grain-
 326 to-grain shearing in saturated, unconsolidated marine sediments. *The*
 327 *Journal of the Acoustical Society of America*, *108*(6), 2796–2815. doi:
 328 <https://doi.org/10.1121/1.1322018>
- 329 Carr, M. H. (1979). Formation of Martian flood features by release of water from
 330 confined aquifers. *Journal of Geophysical Research: Solid Earth*, *84*(B6), 2995–
 331 3007. doi: <https://doi.org/10.1029/JB084iB06p02995>
- 332 Cashman, K. V., & Kauahikaua, J. P. (1997). Reevaluation of vesicle distributions in
 333 basaltic lava flows. *Geology*, *25*(5), 419–422. doi: [https://doi.org/10.1130/0091-7613\(1997\)025\(0419:ROVDIB\)2.3.CO;2](https://doi.org/10.1130/0091-7613(1997)025(0419:ROVDIB)2.3.CO;2)
- 334 Clifford, S. (1986). Mars: Crustal Pore Volume, Cryospheric Depth, and the Global
 335 Occurrence of Groundwater. In *Mars: Evolution of its climate and atmosphere*
 336 (Vol. 599, p. 18).
- 337 Clifford, S. (1997). The origin of the Martian intercrater plains-The role of liquefac-
 338 tion from impact and tectonic-induced seismicity. In *Lunar and planetary sci-*
 339 *ence conference* (Vol. 28, p. 241).
- 340 Davis, R., & Haltigin, T. (2021). International Mars Ice Mapper Mission: The First
 341 Human Exploration Reconnaissance Mission to Mars. In *Lunar and planetary*
 342 *science conference* (p. 2614).
- 343 Day-Lewis, F. D., Singha, K., & Binley, A. M. (2005). Applying petrophysical
 344 models to radar travel time and electrical resistivity tomograms: Resolution-
 345 dependent limitations. *Journal of Geophysical Research: Solid Earth*, *110*(B8).
 346 doi: <https://doi.org/10.1029/2004JB003569>
- 347 Dou, S., Nakagawa, S., Dreger, D., & Ajo-Franklin, J. (2017). An effective-medium
 348 model for P-wave velocities of saturated, unconsolidated saline permafrost.
 349 *Geophysics*, *82*(3), EN33–EN50. doi: <https://doi.org/10.1190/geo2016-0474.1>
- 350 Dundas, C. M., Mellon, M. T., Conway, S. J., Daubar, I. J., Williams, K. E., Ojha,
 351 L., . . . Pathare, A. (2021). Widespread exposures of extensive clean shallow
 352 ice in the midlatitudes of Mars. *Journal of Geophysical Research: Planets*,
 353 *126*(3), e2020JE006617. doi: <https://doi.org/10.1029/2020JE006617>

- 355 Dvorkin, J., & Nur, A. (1996). Elasticity of high-porosity sandstones: Theory for
356 two North Sea data sets. *Geophysics*, *61*(5), 1363–1370. doi: [https://doi.org/](https://doi.org/10.1190/1.1444059)
357 [10.1190/1.1444059](https://doi.org/10.1190/1.1444059)
- 358 Franzson, H., Gufinnsson, G., Helgadóttir, H., & Frolova, J. (2010). Porosity, density
359 and chemical composition relationships in altered Icelandic hyaloclastites.
- 360 Gassmann, F. (1951). Über die elastizität poroser medien. *Vierteljahrsschrift der*
361 *Naturforschenden Gesellschaft in Zurich*, *96*, 1–23.
- 362 Golombek, M., Grott, M., Kargl, G., Andrade, J., Marshall, J., Warner, N.,
363 ... Banerdt, W. (2018). Geology and physical properties investiga-
364 tions by the InSight lander. *Space Science Reviews*, *214*(5), 1–52. doi:
365 <https://doi.org/10.1007/s11214-018-0512-7>
- 366 Golombek, M., Warner, N., Grant, J., Hauber, E., Ansan, V., Weitz, C., ...
367 Banerdt, W. (2020). Geology of the InSight landing site on Mars. *Nature Com-*
368 *munications*, *11*(1), 1–11. doi: <https://doi.org/10.1038/s41467-020-14679-1>
- 369 Hanna, J. C., & Phillips, R. J. (2005). Hydrological modeling of the Martian crust
370 with application to the pressurization of aquifers. *Journal of Geophysical Re-*
371 *search: Planets*, *110*(E1). doi: <https://doi.org/10.1029/2004JE002330>
- 372 Hobiger, M., Hallo, M., Schmelzbach, C., Stähler, S., Fäh, D., Giardini, D., ...
373 Banerdt, W. (2021). The shallow structure of Mars at the InSight landing site
374 from inversion of ambient vibrations. *Nature Communications*, *12*(1), 1–13.
375 doi: <https://doi.org/10.1038/s41467-021-26957-7>
- 376 Kalapodis, N., Kampas, G., & Ktenidou, O.-J. (2020). A review towards the design
377 of extraterrestrial structures: From regolith to human outposts. *Acta Astro-*
378 *nautica*, *175*, 540–569. doi: <https://doi.org/10.1016/j.actaastro.2020.05.038>
- 379 Karl, D., Cannon, K. M., & Gurlo, A. (2021). Review of space resources processing
380 for Mars missions: Martian simulants, regolith bonding concepts and addi-
381 tive manufacturing. *Open Ceramics*, 100216. doi: [https://doi.org/10.1016/](https://doi.org/10.1016/j.oceram.2021.100216)
382 [j.oceram.2021.100216](https://doi.org/10.1016/j.oceram.2021.100216)
- 383 Lewis, K. W., Peters, S., Gonter, K., Morrison, S., Schmerr, N., Vasavada, A. R., &
384 Gabriel, T. (2019). A surface gravity traverse on Mars indicates low bedrock
385 density at Gale crater. *Science*, *363*(6426), 535–537.
- 386 Li, J., Beghein, C., Wookey, J., Davis, P., Lognonné, P., Schimmel, M., ...
387 Banerdt, W. B. (2022). Evidence for crustal seismic anisotropy at the in-
388 sight lander site. *Earth and Planetary Science Letters*, *593*, 117654. doi:
389 <https://doi.org/10.1016/j.epsl.2022.117654>
- 390 Liu, J., Li, H., Sun, L., Guo, Z., Harvey, J., Tang, Q., ... Jia, M. (2021). In-situ re-
391 sources for infrastructure construction on Mars: A review. *International Jour-*
392 *nal of Transportation Science and Technology*. doi: [https://doi.org/10.1016/j](https://doi.org/10.1016/j.ijtst.2021.02.001)
393 [.ijtst.2021.02.001](https://doi.org/10.1016/j.ijtst.2021.02.001)
- 394 Lognonné, P., Banerdt, W., Pike, W., Giardini, D., Christensen, U., Garcia, R. F.,
395 ... Zweifel, P. (2020). Constraints on the shallow elastic and anelastic struc-
396 ture of Mars from InSight seismic data. *Nature Geoscience*, *13*(3), 213–220.
397 doi: <https://doi.org/10.1038/s41561-020-0536-y>
- 398 MacKinnon, D. J., & Tanaka, K. L. (1989). The impacted Martian crust: Struc-
399 ture, hydrology, and some geologic implications. *Journal of Geophysical Re-*
400 *search: Solid Earth*, *94*(B12), 17359–17370. doi: [https://doi.org/10.1029/](https://doi.org/10.1029/JB094iB12p17359)
401 [JB094iB12p17359](https://doi.org/10.1029/JB094iB12p17359)
- 402 Majmudar, T. S., & Behringer, R. P. (2005). Contact force measurements and
403 stress-induced anisotropy in granular materials. *Nature*, *435*(7045), 1079–1082.
404 doi: <https://doi.org/10.1038/nature03805>
- 405 Makse, H. A., Gland, N., Johnson, D. L., & Schwartz, L. (2004). Granular pack-
406 ings: Nonlinear elasticity, sound propagation, and collective relaxation dy-
407 namics. *Physical Review E*, *70*(6), 061302. doi: [https://doi.org/10.1103/](https://doi.org/10.1103/PhysRevE.70.061302)
408 [PhysRevE.70.061302](https://doi.org/10.1103/PhysRevE.70.061302)
- 409 Makse, H. A., Gland, N., Johnson, D. L., & Schwartz, L. M. (1999). Why effective

- 410 medium theory fails in granular materials. *Physical Review Letters*, 83(24),
 411 5070. doi: <https://doi.org/10.1103/PhysRevLett.83.5070>
- 412 Manga, M., & Wright, V. (2021). No Cryosphere-Confined Aquifer Below InSight on
 413 Mars. *Geophysical Research Letters*, 48(8), e2021GL093127. doi: <https://doi.org/10.1029/2021GL093127>
- 414
- 415 Mindlin, R. D. (1949). Compliance of elastic bodies in contact. *American So-*
 416 *ciety of Mechanical Engineers*, 16(3), 259–268. doi: [https://doi.org/10.1115/1](https://doi.org/10.1115/1.4009973)
 417 [.4009973](https://doi.org/10.1115/1.4009973)
- 418 Moitra, P., Horvath, D. G., & Andrews-Hanna, J. C. (2021). Investigating the
 419 roles of magmatic volatiles, ground ice and impact-triggering on a very recent
 420 and highly explosive volcanic eruption on Mars. *Earth and Planetary Science*
 421 *Letters*, 567, 116986. doi: <https://doi.org/10.1016/j.epsl.2021.116986>
- 422 Morgan, G. A., Putzig, N. E., Perry, M. R., Sizemore, H. G., Bramson, A. M., Pe-
 423 tersen, E. I., ... Campbell, B. (2021). Availability of subsurface water-ice
 424 resources in the northern mid-latitudes of Mars. *Nature Astronomy*, 5(3),
 425 230–236. doi: <https://doi.org/10.1038/s41550-020-01290-z>
- 426 Murphy, W. F. (1982). *Effects of microstructure and pore fluids on the acoustic*
 427 *properties of granular sedimentary materials* (Unpublished doctoral disserta-
 428 tion). Stanford University.
- 429 Pan, L., Quantin-Nataf, C., Tauzin, B., Michaut, C., Golombek, M., Lognonné,
 430 P., ... Lucas, A. (2020). Crust stratigraphy and heterogeneities of the first
 431 kilometers at the dichotomy boundary in western Elysium Planitia and impli-
 432 cations for InSight lander. *Icarus*, 338, 113511. doi: [https://doi.org/10.1016/j](https://doi.org/10.1016/j.icarus.2019.113511)
 433 [.icarus.2019.113511](https://doi.org/10.1016/j.icarus.2019.113511)
- 434 Piqueux, S., Buz, J., Edwards, C. S., Bandfield, J. L., Kleinböhl, A., Kass, D. M.,
 435 ... Teams, T. (2019). Widespread shallow water ice on Mars at high latitudes
 436 and midlatitudes. *Geophysical Research Letters*, 46(24), 14290–14298. doi:
 437 <https://doi.org/10.1029/2019GL083947>
- 438 Rivera-Valentín, E. G., Chevrier, V. F., Soto, A., & Martínez, G. (2020). Distribu-
 439 tion and habitability of (meta) stable brines on present-day Mars. *Nature As-*
 440 *tronomy*, 4(8), 756–761. doi: <https://doi.org/10.1038/s41550-020-1080-9>
- 441 Scheller, E., Ehlmann, B., Hu, R., Adams, D., & Yung, Y. (2021). Long-term drying
 442 of Mars by sequestration of ocean-scale volumes of water in the crust. *Science*,
 443 372(6537), 56–62. doi: DOI:10.1126/science.abc7717
- 444 Sharma, S. S., & Fahey, M. (2003). Degradation of stiffness of cemented cal-
 445 careous soil in cyclic triaxial tests. *Journal of Geotechnical and Geoen-*
 446 *vironmental Engineering*, 129(7), 619–629. doi: [https://doi.org/10.1061/](https://doi.org/10.1061/(ASCE)1090-0241(2003)129:7(619)
 447 [\(ASCE\)1090-0241\(2003\)129:7\(619\)](https://doi.org/10.1061/(ASCE)1090-0241(2003)129:7(619)
- 448 Smrekar, S. E., Lognonné, P., Spohn, T., Banerdt, W. B., Breuer, D., Christensen,
 449 U., ... Wieczorek, M. (2019). Pre-mission InSights on the interior of
 450 Mars. *Space Science Reviews*, 215(1), 1–72. doi: [https://doi.org/10.1007/](https://doi.org/10.1007/s11214-018-0563-9)
 451 [s11214-018-0563-9](https://doi.org/10.1007/s11214-018-0563-9)
- 452 Spohn, T., Hudson, T. L., Witte, L., Wippermann, T., Wisniewski, L., Kedziora, B.,
 453 ... Grygorczuk, J. (2022). The InSight-HP3 mole on Mars: Lessons learned
 454 from attempts to penetrate to depth in the Martian soil. *Advances in Space*
 455 *Research*, 69(8), 3140-3163. doi: <https://doi.org/10.1016/j.asr.2022.02.009>
- 456 Squyres, S., Aharonson, O., Arvidson, R., Bell, J., Christensen, P., Clark, B., ...
 457 Tosca, N. (2006). Bedrock formation at Meridiani Planum. *Nature*, 443(7107),
 458 E1–E2. doi: <https://doi.org/10.1038/nature05212>
- 459 Squyres, S., Arvidson, J., Bell, J., Brückner, N., Cabrol, W., Calvin, M., ... Yen,
 460 A. (2004). The opportunity rover’s athena science investigation at merid-
 461 iani planum, mars. *Science*, 306(5702), 1698–1703. doi: doi:10.1126/
 462 [science.1106171](https://doi.org/10.1126/science.1106171)
- 463 Suazo, G., Fourie, A., & Doherty, J. (2017). Cyclic shear response of cemented paste
 464 backfill. *Journal of Geotechnical and Geoenvironmental Engineering*, 143(1),

- 465 04016082. doi: [https://doi.org/10.1061/\(ASCE\)GT.1943-5606.0001581](https://doi.org/10.1061/(ASCE)GT.1943-5606.0001581)
- 466 Sun, V. Z., Stack, K. M., Kah, L. C., Thompson, L., Fischer, W., Williams, A. J.,
467 ... VanBommel (2019). Late-stage diagenetic concretions in the Murray for-
468 mation, Gale crater, Mars. *Icarus*, *321*, 866–890. doi: [https://doi.org/10.1016/j.
469 j.icarus.2018.12.030](https://doi.org/10.1016/j.icarus.2018.12.030)
- 470 Suzuki, M., Umezaki, T., & Takahara, H. (2012). Fast and cyclic shearing of ce-
471 mented sand in Earthquake induced landslide. In *Proc. 15th world conference
472 on earthquake engineering, lisboa.*
- 473 Tanaka, K. L., Skinner Jr, J. A., Dohm, J. M., Irwin III, R. P., Kolb, E. J.,
474 Fortezzo, C. M., ... Trent, M. (2014). Geologic map of Mars.
- 475 Vanorio, T., Prasad, M., & Nur, A. (2003). Elastic properties of dry clay mineral
476 aggregates, suspensions and sandstones. *Geophysical Journal International*,
477 *155*(1), 319–326. doi: <https://doi.org/10.1046/j.1365-246X.2003.02046.x>
- 478 Walton, K. (1987). The effective elastic moduli of a random packing of spheres.
479 *Journal of the Mechanics and Physics of Solids*, *35*(2), 213–226. doi: [https://
480 doi.org/10.1016/0022-5096\(87\)90036-6](https://doi.org/10.1016/0022-5096(87)90036-6)
- 481 Wang, C.-y., Manga, M., & Wong, A. (2005). Floods on Mars released from ground-
482 water by impact. *Icarus*, *175*(2), 551–555. doi: [https://doi.org/10.1016/j.
483 icarus.2004.12.003](https://doi.org/10.1016/j.icarus.2004.12.003)
- 484 Warner, N., Golombek, M., Ansan, V., Marteau, E., Williams, N., Grant, J., ...
485 Banks, M. (2022). In Situ and Orbital Stratigraphic Characterization of the
486 InSight Landing Site—A Type Example of a Regolith-Covered Lava Plain on
487 Mars. *Journal of Geophysical Research: Planets*, *127*(4), e2022JE007232. doi:
488 <https://doi.org/10.1029/2022JE007232>
- 489 Wernicke, L. J., & Jakosky, B. M. (2021). Martian hydrated minerals: A significant
490 water sink. *Journal of Geophysical Research: Planets*, *126*(3), e2019JE006351.
491 doi: <https://doi.org/10.1029/2019JE006351>
- 492 Wright, V., & Hornbach, M. (2021). The effects of 180 years of aging on the phys-
493 ical and seismic properties of partially saturated sands. *Journal of Geophysical
494 Research: Solid Earth*, *126*(6), e2020JB021341. doi: [https://doi.org/10.1029/
495 2020JB021341](https://doi.org/10.1029/2020JB021341)
- 496 Zeghal, M., & El Shamy, U. (2008). Liquefaction of saturated loose and cemented
497 granular soils. *Powder Technology*, *184*(2), 254–265. doi: [https://doi.org/10.
498 1016/j.powtec.2007.11.032](https://doi.org/10.1016/j.powtec.2007.11.032)
- 499 Zimmer, M. A., Prasad, M., Mavko, G., & Nur, A. (2007). Seismic velocities of un-
500 consolidated sands: Part 1—Pressure trends from 0.1 to 20 MPa. *Geophysics*,
501 *72*(1), E1–E13. doi: <https://doi.org/10.1190/1.2399459>
- 502 Zong, J., Stewart, R. R., Dyaur, N., & Myers, M. T. (2017). Elastic properties of
503 rock salt: Laboratory measurements and Gulf of Mexico well-log analysis. *Geo-
504 physics*, *82*(5), D303–D317. doi: <https://doi.org/10.1190/geo2016-0527.1>